Isotopic composition of convective rainfall in the inland tropics of Brazil

Vinicius dos Santos[1], Didier Gastmans[1], Ana María Durán-Quesada[2], Ricardo Sánchez-Murillo[3], Kazimierz Rozanski[4], Oliver Kracht[5] and Demilson de Assis Quintão[6].

[1]São Paulo State University (UNESP), Environmental Studies Center. Av. 24ABased, 1515, Bela Vista, 13.506-900, Rio Claro, São Paulo, Brazil. vinicius.santos16@unesp.br; didier.gastmans@unesp.br

[2]Escuela de Física & Centro de Investigación en Contaminación Ambiental & Centro de Investigaciones Geofísicas, Universidad de Costa Rica, San José 11501, Costa Rica. ana.duranquesada@ucr.ac.cr

[3]University of Texas at Arlington, Department of Earth and Environmental Sciences, 500 Yates Street, Arlington, Texas 76019, USA. ricardo.sanchezmurrillo@uta.edu

[4] Faculty of Physics and Applied Computer Science, AGH University of Science and Technology, al. Mickiewicza 30, 30-059 Krakow, Poland. rozanski@agh.edu.pl

[5]International Atomic Energy Agency, Isotope Hydrology Section, Vienna International Centre, P. O. Box 100, 1400 Vienna, Austria. O.Kracht@iaea.org

[6]São Paulo State University (UNESP), IPMet/Science College, Est. Mun. José Sandrin IPMET, S/N, 17.048-699, Bauru, São Paulo, Brazil. demilson.quintao@unesp.br

Correspondence to: Didier Gastmans (didier.gastmans@unesp.br)

Abstract. The tropical central-southern part of Brazil (CSB) is characterized by strong convective systems bringing generous water supply for agro-industrial activities but also pose flood risks for large cities. Here, we present high-frequency (2-10 minutes) rainfall isotopic compositions to better understand those systems, with a total of 90 intra-event samples collected during the period 2019-2021. Combining intra-event and inter-event analysis it is explained how regional and local meteorological processes control the isotope variability within 8 convective rainfall events. While convective activity, associated with outgoing longwave radiation (OLR) and moisture transport, evaluated from Hysplit modelling and ERA-5 eastward vapor flux, modulate the seasonal rainwater isotopic composition. Low $\delta^{18}O$ values (median <-6.8‰) were observed during summer, when lower OLR and predominantly moisture influence from Amazon Forest), while high values (median >-4.2‰) during autumn and spring, when higher OLR and moisture from Atlantic Ocean and South Brazil are acting. A semi-quantitative evaporation model evaluated local influences in summer convective events revealing distinct isotope characteristics between day (high $\delta^{18}O$, low *d*-excess and substantial evaporation) and night (low $\delta^{18}O$, high *d*-excess and negligible evaporation). Our results offer a new framework of key drivers controlling the isotopic variability of rainfall in tropical South America that must be considered in future studies of convective systems across the tropics.

1 Introduction

The central-southern part of Brazil (CSB) is the main contributor to the Brazilian economy, with agriculture and industry as leading activities (Zilli et al., 2017). These sectors strongly depend on rainfall seasonality for irrigation and hydropower supply (Luiz Silva et al., 2019). Suggested changes in frequency of heavy and extreme rainfall events in future climate scenarios (Marengo et al., 2020; Donat et al., 2013; IPCC, 2021) may represent a serious threat to regional economic activities and electricity generation. Similarly, climate projections also suggest that enhancement of heavy rainfall events will aggravate the occurrence of both floods and landslides across vulnerable areas (Marengo et al., 2020), whose total cost has risen to US$ 41.7 billion in the past 50 years (Marengo et al., 2020; World Meteorological Organization, 2021).

Extreme rainfall events are related to the convective systems (CS), characterized by strong vertical development in the form of *cumulus-nimbus* and *cumulus congestus* (convective clouds) and low-level divergence (stratiform clouds) (Siqueira et al., 2005; Machado and Rossow, 1993; Zilli et al., 2017; Houze, 1989, 2004), commonly refer to as convective and stratiform rainfall, that account for 45% and 46% of the total rainfall in South America, respectively (Romatschke and Houze, 2013). These rainfall types have recently been postulated as a major driver explaining variations in stable isotope composition of precipitation across the tropics (Zwart et al., 2018; Sánchez-Murillo et al., 2019; Sun et al., 2019; Han et al., 2021; Aggarwal et al., 2016). Specifically, the role of tropical convection in formation of the isotopic composition of rainfall has been discussed in the context of so-called amount effect (heavy isotope contents of tropical precipitation decrease as the amount of local precipitation increases) (Dansgaard, 1964; Hu et al., 2018; Kurita, 2013; Rozanski et al., 1993; Winnick et al., 2014; Tharammal, T., G. Bala, 2017).

Previous studies used satellite retrievals of atmospheric water vapor isotopic composition to better understand convective processes in other regions (Lawrence et al., 2004; Worden et al., 2007; Kurita, 2013). They showed the links between the structure and depth of convective systems as well as variations in the isotopic composition of local vapor (e.g. Lekshmy et al., 2014; Vuille et al., 2003; dos Santos et al., 2022). Despite these advances, to date only few studies have examined the rainfall isotopic composition in the light of diurnal variations in convective activity of tropical atmosphere (Munksgaard et al., 2020; Moerman et al., 2013).

Diurnal variations in heating of the surface intensify convection processes, generating short-lived events that can occur in consecutive days across the tropics (Romatschke and Houze, 2013, 2010). These events are characterized by a diurnal cycle and notable differences in: (i) rainfall intensity, (ii) vertical extent of convective cores between deep and shallow convection, and (iii) life cycle of these events in mesoscale convective systems (MCSs) (Schumacher and Houze, 2003; Romatschke and Houze, 2013, 2010). Convective events account for a significant proportion of annual rainfall and are linked with extreme events over the land, with most intense events occurring in the afternoon (Schumacher and Houze, 2003; Kurita, 2013; Wang and Tang, 2020). High-frequency rainfall sampling strategies during the occurrence of convective events are needed to capture the diurnal heating cycle and associated variations in the isotopic signatures of convective rainfall.

High-frequency rainfall sampling and analyses of stable isotope ratios has been used to better understand the evolution of large weather systems such as tropical cyclones and typhoons (Sun et al., 2022; Sánchez-Murillo et al., 2019; Han et al., 2021), squall lines (Taupin et al., 1997; Risi et al., 2010; Tremoy et al., 2014) and local evaporation effects (Graf et al., 2019; Aemisegger et al., 2015; Lee and Fung, 2008). This high-resolution isotope information provided a better insight into the development of weather systems and cloud dynamics, both responsible for changes in the rain type, intensity, and inherent isotope variability during rainfall events (Coplen et al., 2008; Muller et al., 2015; Celle-Jeanton et al., 2004). Nevertheless, high-frequency isotope sampling of rainfall has been limited across the tropics, despite convective activity being significant in this region.

Using high-frequency rainfall sampling strategy we focus here on processes controlling isotopic composition of convective rainfall, which are of local (below-cloud evaporation and isotope exchange processes, vertical structure of rainfall, cloud top over sampling site, and others) and regional (moisture origin/transport, regional atmospheric circulation). We combine high-frequency rainfall sampling with ground-based observational data (Micro Rain Radar, and automatic weather station) with satellite imagery (GOES-16), ERA-5 reanalysis products and HYSPLIT trajectories to characterize convective rainfall collected over the inland tropics of Brazil.

2 Data and Methods

2.1 Sampling site and weather systems

The rainfall sampling site was localized in Rio Claro city, São Paulo State (Fig. 1a). The station (-22.39°S, -47.54°W, 670 m.a.s.l.) belongs to Global Network of Isotopes in Precipitation network (GNIP) and is influenced by weather systems responsible for rainfall variations and seasonality linked to the regional atmospheric circulations of CSB region. The rainfall seasonality over CSB is associated with: (i) frontal systems (FS), represented mainly by cold fronts from southern South America acting all the year, and (ii) the South Atlantic Convergence Zone (SACZ) during austral summer (December to March) (Kodama, 1992; Garreaud, 2000) (Fig. 1b). These synoptic features are mostly responsible for the development of CS (Romatschke and Houze, 2013; Siqueira et al., 2005; Machado and Rossow, 1993) (Fig. 1c), and were captured during their passage over the Rio Claro station.

2.2 Rainfall sampling and isotope analyses

High-frequency sampling of rainfall events was done manually with the aid of passive collector (ca. 2 to10 minutes intervals) from September 2019 to February 2021, except for April, July, and August (during winter 2020), when no rainfall was observed in the study area. Due to the difficulties of manual sampling and uncertainties involved in forecast of rainfall occurrences for one point, rainfall events were collected randomly during the monitoring period. Covid-19 restricted access at the university,

which resulted in fewer rainfall events sampled, mainly at night during spring-2020. The rainfall samples collected in this study generally do not represent consecutive pairs of day-night data during the same day. Daytime data are related to rainfall samples collected at Rio Claro station from 07:00 to 18:59 local time (10:00-21:59 UTC) whereas night-time data represent the period 19:00-06:59 local time (22:00-09:59 UTC). In total, 90 samples representing eight convective events (3 night-time events and 5 day-time events) have been collected. The collected samples were transferred to the laboratory and stored in 20 ml HDPE bottles at reduced temperature (+4°C). In parallel to high-frequency sampling, monthly cumulative rainfall samples were also collected at the Rio Claro site during the study period as a contribution to the GNIP network, using the methodology recommended by the International Atomic Energy Agency (IAEA, 2014).

2.3 Isotope analyses

Rainfall samples were analysed for stable isotope composition using Off-Axis Integrated Cavity Output Spectroscopy (Los Gatos Research Inc.) at the Hydrogeology and Hydrochemistry laboratory of UNESP's Department of Applied Geology and at the Chemistry School of the National University (Heredia, Costa Rica). All results are expressed in per mil relative to Vienna Standard Mean Ocean Water (V-SMOW). The certified calibration standards used in UNESP were USGS-45 (δ^2H = −10.3‰, $\delta^{18}O$ = −2.24‰), USGS-46 (δ^2H = −236.0‰, $\delta^{18}O$ = −29.80‰), including one internal standard (Cachoeira de Emas - CE – δ^2H = −36.1‰, $\delta^{18}O$ = −5.36‰). USGS standards were used to calibrate the results on the V-SMOW2-SLAP2 scale, whereas CE was used for memory and drift corrections. In Costa Rica laboratory, the certified standards MTW (δ^2H = −130.3‰, $\delta^{18}O$ = −16.7‰), USGS45 (δ^2H = −10.3‰, $\delta^{18}O$ = −2.2‰), and CAS (δ^2H = −64.3‰, $\delta^{18}O$ = −8.3‰) were used to correct the measurement results for memory and drift effects and to calibrate them on the V-SMOW2-SLAP2 scale (García-Santos et al., 2022). The analytical uncertainty (1σ) was 1.2‰ for δ^2H and 0.2‰ for $\delta^{18}O$ for UNESP analysis and 0.38‰ for δ^2H and 0.07‰ for $\delta^{18}O$ for Costa Rica analysis. Deuterium excess (*d*-excess) was calculated as: *d*-excess = $\delta^2H - 8*\delta^{18}O$ (Dansgaard, 1964). Its uncertainty 1(σ) resulting from the uncertainties of the isotope analyses was equal 1.33 and 0.43‰, respectively. This secondary isotope parameter was used to interpret the influence of moisture origin/transport (Sánchez-Murillo et al., 2017; Froehlich et al., 2002) and to quantify below-cloud processes (e.g. Jeelani et al., 2018; Graf et al., 2019; Aemisegger et al., 2015).

2.4 Meteorological data

Automatic Weather Station (AWS) Decagon Em50 (METER) was installed near the Micro Rain Radar (MRR) (METEK) at 670 m.a.s.l, in immediate vicinity of the rainfall collection site. Meteorological data were recorded at 1 min intervals for rain rate (AWS RR, $mm.min^{-1}$), air temperature (T, °C) and relative humidity (RH, %). The MRR data for reflectivity (Z, dBZ), and fall velocity (w, $m.s^{-1}$) were also recorded at 1 min intervals. MRR parameters correspond to the mean values measured at the elevation between 150 and 350 meters above the local ground. MRR operated at a frequency of 24.230 GHz,

modulation of 0.5 – 15 MHz according to the height resolution mode. For this work, different height resolutions (31 range bin) were tested, 150m, 200m, 300m and 350m, resulting in vertical profiles of 4650m, 6200m, 9300m and 10.850m, respectively (Endries et al., 2018). The MRR data used in the following discussion are the near-surface data (first measurement from 150m to 350m). The MRR vertical profile (from 150m to 10,850m) was used to classify and visualize the radar echoes. Lifting Condensation Level (LCL, meters) was computed from AWS RH and T, using expression proposed by Soderberg et al. (2013).

GOES-16 imagery (https://home.chpc.utah.edu/~u0553130/Brian_Blaylock/cgi-bin/goes16_download.cgi) was used to identify the convective nuclei of the cloud-top (10.35-μm, Band-13) and brightness temperature (BT), at 10 min intervals during the sampling period (Ribeiro et al., 2019; Schmit et al., 2017). The 10.35-μm BT is often used to estimate the convective cloud depth, since the lower BT is linked to deeper cloud tops (Adler and Fenn, 1979; Roberts and Rutledge, 2003; Adler and Mack, 1986; Ribeiro et al., 2019; Machado et al., 1998).

The weather systems (Frontal, instabilities and low pressure) were defined according to the synoptic chart (https://www.marinha.mil.br/chm/dados-do-smm-cartas-sinoticas/cartas-sinoticas) and meteorological technical bulletin of the Center for Weather Forecast and Climatic Studies of the National Institute of Space Research (CPTEC/INPE: (http://tempo.cptec.inpe.br/boletimtecnico/pt) that used information of numerical model, modern observation systems, automatic weather stations, satellite and radar images, reanalysis data and regional atmospheric models, such as the Brazilian Global Atmospheric Model and ETA model.

2.5. Hysplit modelling and reanalysis data

The origin of air masses and moisture transport to the Rio Claro site were evaluated using the HYSPLIT (Hybrid-Single Particle Langragian Integrated Trajectory) modelling framework (Stein et al., 2015; Soderberg et al., 2013). The trajectories of the air masses were estimated for 240 hours prior to rainfall onset, considering the estimated time of residence of the water vapor (Gimeno et al., 2010, 2020; van der Ent and Tuinenburg, 2017). Start time of trajectories was the same as the start time of rainfall events. The trajectories were computed using NOAA′s meteorological data (global data assimilation system, GDAS: 1 degree, global, 2006-present), with ending elevations of the trajectories at 1500 m above the surface, taking into account the climatological height of the Low Level Jet, within 1000–2000 m (Marengo et al., 2004). Ten-day trajectories representing convective events were calculated as trajectory ensembles, each consisting of twenty-seven ensemble members released at start hour of convective rainfall sample collection. Ensembles were produced by varying the initial trajectory wind speeds and pressures, according to the HYSPLIT ensemble algorithm, in order to account for the uncertainties involved in the simulation of individual backward trajectories (Jeelani et al., 2018).

Reanalysis data were used to better understand the influence of atmospheric circulation on isotopic composition of rainfall at the study area. ERA-5 climatology (https://cds.climate.copernicus.eu/cdsapp#!/search?type=dataset) was used to generate plots of hourly vertical integral of eastward water vapor flux during convective events sampled. The Global Modelling and Assimilation Office (GMAO) data (MERRA-2, 1 hour, 0.5 x 0.625 degree, V5.12.4 -

https://goldsmr4.gesdisc.eosdis.nasa.gov/data/MERRA2/M2T1NXFLX.5.12.4/) were used for calculations of latent heat flux (LHF), and Aqua/AIRS L3 Daily Standard Physical Retrieval (AIRS-only) 1 degree x 1 degree V7.0, Greenbelt, MD, USA, Goddard Earth Sciences Data and Information Services Center (GES DISC) data were used for average outgoing longwave radiation (OLR) (https://disc.gsfc.nasa.gov/datasets/AIRS3STD_7.0/summary). OLR values below 240W.m^{-2} indicate organized deep convection (Gadgil, 2003). Global Land Data Assimilation System Version 2 (GLDAS-2) Noah Land Surface Model L4 3 hourly 0.25 x 0.25 degree V2.1, Greenbelt, Maryland, USA, Goddard Earth Sciences Data and Information Services Center (GES DISC) were used for calculations of evapotranspiration (https://disc.gsfc.nasa.gov/datasets/GLDAS_NOAH025_3H_2.1/summary). A 10-day mean evapotranspiration values (mm) were computed based on the back hour (240 hours) and coordinates (latitude e longitude) of HYSPLIT trajectories.

2.6 Identification of convective rainfall events

In general, identification of convective precipitation systems was based on the vertical structure of the given precipitation system (lack of the melting layer and bright band - BB) in the radar profiles featuring high reflectivity values (Z >38 dBZ) (Houze, 1993, 1997; Steiner and Smith, 1998; Rao et al., 2008; Mehta et al., 2020; Endries et al., 2018) and satellite imagery (Vila et al., 2008; Ribeiro et al., 2019; Siqueira et al., 2005; Machado et al., 1998). Consequently, convective rainfall was defined in this study by (i) convective cloud nuclei observed in GOES-16 imagery, (ii) no BB detected, (iii) Z > 38dBZ nearto the surface and (iv) rainfall intensity (AWS) of at least 10mm.h^{-1} (Klaassen, 1988) (Fig. 1c,d). The convective nuclei were identified using GOES-16 imagery, determined as a contiguous area of at least 40 pixels with BT lower than 235K (≤-38°C) over Rio Claro station, according to previous studies (Ribeiro et al., 2019).

3 Results and Discussion

A complete database comprising the results of high-frequency sampling of convective rainfall events occurring during the study period at the Rio Claro site (isotope characteristics of rainfall as well as selected meteorological parameters characterizing these events) can be found et: (dos Santos et al., 2023). Table 1 contains median values of isotope and meteorological parameters for the studied rainfall events, separated into night-time and day-time categories.

3.1 Seasonal variations of isotope characteristics and selected meteorological parameters of monthly rainfall

Seasonal variations of the isotopic composition of monthly cumulative precipitation and selected meteorological parameters (latent heat flux, outgoing longwave radiation flux (OLR), monthly amount of rainfall) recorded at the Rio Claro site during the study period (September 2019 – February 2021), are presented in Fig. 2. The monthly values of meteorological parameters were split in Fig. 2 into day and night fraction. Superimposed on monthly values of $\delta^{18}O$ presented in Fig. 2a are monthly

averages of this parameter derived from high-frequency sampling of the convective events. Although they do not cover uniformly the presented study period, it is clear that they follow the seasonal variations of $\delta^{18}O$ derived for monthly cumulative precipitation samples. A sharp seasonal contrast in the isotopic composition of rainfall for rainy and dry season (austral summer and winter, respectively) is apparent in Fig. 2a. The Local Meteoric Water Lines (LMWL) for the Rio Claro site based on monthly cumulative and high-frequency samples (Fig 3) cannot be directly compared because of incomplete coverage of rainfall in the given month by the high-frequency sampling. The high-frequency sampling strategy employed in the study was aimed to capture specific rainfall events for each season (cf. Fig. 2a).

The seasonal and day-night fluctuations of convective activity characterized by latent heat flux and OLR flux (Fig. 2b,c) and rainfall amount (Fig. 2d) were observed during the study period, resulting in different conditions for occurrence of convective events and high-frequency sampling of rainfall. Contrary to summer, during autumn and spring, latent heat fluxes were lower (Fig. 2b) and OLR was higher (Fig. 2c), which in turn may have inhibited convective development related to thermal forcings (Houze, 1997, 1989).

3.2 Intra-event variability of the isotope and meteorological parameters

Temporal evolution of isotope characteristics **(**$\delta^{18}O$, *d*-excess) and selected meteorological parameters (brightness temperature, MRR reflectivity and rainfall amount) of convective rainfall events sampled and analyzed in this study is presented in Fig. 4.

In this figure, radar ecos for all sampled events. The emphasizes the absence of pattern in measured values for the reflectivity (Zc) on the vertical profile (Fig. 4a-b, g-h, m-n, s-t), only near surface higher values were observed (from 2km to 200m), indicating an increase in raindrop size, hence an increase in Z values and rain rates. Despite the similar vertical structure, the temporal evolution was quite distinct between the events, according to the season when the event was collected. The brightness temperature of GOES-16 (BT) has distinct temporal distributions between events (Fig. 4e-f, k-l, q-r, w-x), despite the no relationship observed between variations of BT and a change in isotope values.

For the events collected during the summer, 2020/02/01-day (Fig. 4c,e) and 2020/01/30-night (Fig. 4d,f) the duration were similar (20min and 25min, respectively), similar temporal $\delta^{18}O$ evolution (-10.29 ~ -10.07‰ (stationary trend) and -10.13 ~ -9.91‰ (little increasing trend) and similar rain rates trends (2.8 ~ 0.1mm and 4.4 ~ 0.1mm), respectively. Contrary to the 2021/02/24-day (Fig. 4i, k) and 2020/02/10-night (Fig. 4j, l) events, that had similar longer duration (02h01min and 02h39min, respectively), however, had distinct variations of $\delta^{18}O$ and rain rates (-7.60 ~ -4.47‰ (increasing trend) and -12.35 ~ -13.99‰ (decreasing trend) and 2.6 ~ 0.3mm and 0.6 ~ 0.6mm, respectively), illustrate the remarkably difference between day (enriched) and night (depleted) isotopic composition. Lower *d*-excess values were observed on 2021/02/24 (9.3 ~ 1.2‰) 2020/02/01 (11.3 ~ 7.0‰) and 2020/02/10 (21.4 ~ 4.8‰). While for 2020/02/01 and 2020/02/10 these lower *d*-excess values have been observed at the end of event, when rain rates were lower (0.01mm and 0.8mm, respectively), indicating the residual precipitation, as the rainfall dissipates (Celle-Jeanton et al., 2004), on 2021/02/24 lower *d*-excess values were observed in some parts of the event,

associated to lower Z values (from 16:38 to 17:15). The differences on isotopic composition and a possible effect to below-cloud evaporations for these events are detailed discussed in section 3.4.

For the events collected during the autumn (2020/06/09 (Fig. 4o) and 2020/05/23 (Fig. 4p) values and variations on $\delta^{18}O$ were similar (-3.67 ~ -2.76‰ and -2.67 ~ -2.75‰), the first event showed a little decreasing trend, while the second is stationary. On the other hand, 2020/06/09 and 2020/05/23 *d*-excess values (25.4 ~ 6.3‰ and 16.7 ~ 19.0‰, respectively), trends (w-shaped and stationary), RR (6.2 ~ 0.01mm and 2.6 ~ 0.2mm), BT (-55 ~ -35°C and -60 ~ -52°C) and vertical structure variable (two peaks of higher Z values near-surface (4m) and one peak oh high Z values at start (Fig. 4n), respectively. Despite the decrease of BT values along the time observed in the 09/06/2020 event, lower *d*-excess values and a slight $\delta^{18}O$ increase have been observed during the peak of RR. These changes on isotope distribution could be related to the passage of convective development zones during the event evolution (Risi et al., 2010), from a strong convective activity, corroborated by lower BT values (-55 ~ -52°C) and higher Z (between 17:04 and 14:44), to convection transition activity, represented by an increase on BT (-51 ~ -48°C) and lower Z (between 17:46 to 18:09) and finally, to lower convective development, characterized by higher BT values (>-45°C), and higher Z (between 18:12 to the end).

Spring convective events, collected on 2019/11/05 (Fig. 4u,) and 2020/11/18 (Fig. 4v), have shown opposite isotope variations (-3.00 ~ -1.78‰ and -2.76 ~ -5.40‰) and trends (increasing and decreasing, respectively). Values of RR, normally higher, BT, normally lower, did not present relationship with the isotopic variation (Fig. 4w, x). Values of *d*-excess were stationary on 2019/11/05 event (28.0 ~ 21.0‰), while presented an increase trend during the event collected on 2020/11/18 (10.2 ~ 23.1‰). Any value of *d*-excess were lower than 10‰. The vertical profile of Z is quite distinct between spring events (Fig. 4s, t), higher Z values near-surface was observed at the start and lower at the end of 2019/11/05, while on 2020/11/18 a strong peak of Z occurred at the end (between 16:15 and 16:25). These temporal evolutions in the vertical profile of events 2019/11/05 and 2020/11/18 illustrate the opposite isotope trends (increasing and decreasing, respectively) generally related to the fast condensation and rainfall formation due to the strong updrafts (e.g. Sodemann, 2006; Gedzelman and Lawrence, 1990) and isotopic equilibrium between droplets and vapor (e. g. Celle-Jeanton et al., 2004; Barras and Simmonds, 2009; Muller et al., 2015), respectively.

The weather systems (indicated for each rainfall event in Fig. 6) interacting with the moisture available producing the rainfall systems. A large influence of the cold fronts was observed before, during and after their passage over the study area. Convective rainfall directly formed by the frontal systems (cold front acting at the study area) for 2019/11/05, 2020/11/18, 2020/05/23 and 2020/02/01 events had distinct isotope trends (increasing, decreasing, stationary and stationary), respectively. The instability (frontal) system (when a cold front is localized in the south of Brazil and generates changes in the regional atmosphere over São Paulo state) occurred for 2020/06/09 (decreasing) and 2021/02/24 (increasing trend) events, while thermal instability formed by atmospheric ascend due to surface heat in inland Brazil of 2020/01/30 (little increasing trend), and low pressure (frontal) system (when the cold front is localized in the Atlantic Ocean near Southeast portion of Brazil and interacts with regional atmosphere) for 2020/02/10 (decreasing trend).

The large diversity of trends is quite different observed in previous studies of cold fronts in mid-latitudes, generally related to the V-shaped and strong δ depletion (e. g. Aemisegger et al., 2015; Gedzelman and Lawrence, 1990; Celle-Jeanton et al., 2004; Muller et al., 2015). Apparently, for intra-events presented here, it is difficult to relate the contribution of weather systems control of isotopic variability, due to the different conditions of temperature, moisture available and convective activity (lower during autumn-spring and higher during summer in Fig. 2) along the seasons. Perhaps, which contributes to connecting regional processes to isotope variations, mainly the large *d*-excess distributions, is the associate origin and transport with inter-event evaluation, illustrated in Fig. 5 and 6 detailed in the 3.3. section.

3.3. Inter-event variability of the isotope and meteorological parameters

Figure 5 shows Hysplit ensemble trajectories calculated for each analyzed rainfall event, divided into seasons (summer, autumn and spring). It is clear from Table 1 and Fig. 5 that three summer events, undoubtedly associated with moist air masses arriving from the Amazon basin (2020/02/10, 2020/02/01 and 2020/01/30), have remarkably similar isotope and meteorological characteristics (δ^2H, $\delta^{18}O$, *d*-excess, RH), irrespectively whether they are day-time or night-time events. In contrast, the day-time event which occurred on 2021/02/24 and revealed higher δ values, lower *d*-excess and lower relative humidity, was fed by moisture of Atlantic origin (Fig. 5a).

The estimated vertical integral eastward vapor fluxes using data from ERA-5 (Fig. 6) combined with Hysplit air masses backward trajectories, shows clearly the predominant influence of Amazon moisture for 2020/02/01, 2020/01/30 and 2020/02/10 convective events, representing summer events (Fig. 6a, b, d), marked by the negative values for vertical vapor fluxes (< -250 kg m^{-1} s^{-1}) over the Amazon basin (indicating the direction of moisture vapor flux from the Ocean to Amazon Forest) and positive values (> ~500 kg m^{-1} s^{-1}) over the central-southern portion of Brazil (indicating the direction of vapor flux from Amazon basin with pathways over the study area to the Atlantic Ocean). The higher positive values (~750 kg m^{-1} s^{-1} in red color in Figure 6a, b, d) illustrate the acts of cold fronts between the continental portion and the Atlantic Ocean. This regional pattern was not observed during on 2021/02/24, eastward vapor flux is positive and has high values over the Atlantic Ocean (250 ~ 750 kg m^{-1} s^{-1}), corroborating the distinct moisture transport, δ values and relative humidity values.

The two events representing autumn season (2020/05/23 - night-time event and 2020/06/09 – day-time event) were associated with mean trajectories similar to those calculated for the spring season (Fig. 5b). In this case the continental origin of moist air masses (south-western Brazil) is more pronounced (2020/05/23), whereas the Amazon-type trajectory starts in southern Atlantic and does not reach the boundary of the rainforest. In fig. 6, the eastward vapor flux illustrates the continental origin of moist air masses on 2020/05/23 and Atlantic origin for the 2020/06/09. While on 2020/05/23 negative values (-500 ~ -250 kg m^{-1} s^{-1}) were observed in south-western Brazil (indicating transport from the Atlantic Ocean to the continent), which formed a vapor flux of positive values (500 ~ 750 kg m^{-1} s^{-1}) from western Brazil to the study area (Figure 6f), on 2020/06/09 slight negative values (-250 ~ 0 kg m^{-1} s^{-1}) of eastward vapor flux over Amazon basin indicate the decrease of rainforest

moisture flux, positive vapor flux values (250 ~ 500 kg m^{-1} s^{-1}) over the western portion of continental Brazil and study area corroborate that the trajectory started from Atlantic Ocean to arrive directly over the Rio Claro station (Fig. 5b and Fig. 6e).

Finally, two day-time events available for the spring season (Fig. 5c) also reveal contrasting origin of moisture. The mean trajectory for the 2020/11/18 belongs clearly to the Amazon category, although it is passing only over the south-eastern boundary of the Amazon rainforest and has much shorter extension when compared with the Amazon trajectories observed during the summer season, thus positive values of eastward vapor flux (250 ~ 750 kg m^{-1} s^{-1}) are not distribution along from Amazon basin to Atlantic Ocean as typically observed previously (Fig. 6h). The mean trajectory for the second event (2019/11/05) and higher positive eastward vapor flux (> 500 kg m^{-1} s^{-1}, Fig. 6g) are circling around the Rio Claro, pointing to the continental origin (southern Brazil) of moist air masses responsible for this event.

It is apparent from Fig. 5a and Table 1 that three summer events mentioned above (2020/02/10, 2020/02/01 and 2020/01/30) are very consistent in terms of the length and shape of backward trajectories of moist air masses, as well as isotope characteristics of the rainfall events produced from those air masses. The mean δ^2H, $\delta^{18}O$ and *d*-excess values for those three events are equal -76.6, -11.4, 15.5‰, respectively. The ground-level relative humidity is also consistent (mean value 94%, range ca. 5%). Autumn and spring events also reveal remarkable degree of consistency in terms of origin of moisture and isotope characteristics of rainfall (cf. Table 1 and Fig, 5b,c). The mean δ^2H, $\delta^{18}O$ and *d*-excess values are equal -6.4, -3.4, 19.1‰, respectively. Mean relative humidity is equal 90.8%. Those dramatic differences between δ values of convective rainfall sampled during summer months and that sampled during spring and autumn (ca. 8‰ for $\delta^{18}O$ and 70‰ for δ^2H), generated under similar thermal conditions in the region, call for explanation. Also, substantially higher mean *d*-excess value for spring and autumn events (the difference with respect to summer mean value equal 3.6‰) needs to be understood.

We suggest that isotope characteristics of convective events investigated in this study (both the δ values and the *d*-excess) are controlled by three major factors: (i) the origin of moisture and the degree of rainout of moist air masses responsible for precipitation over the Rio Claro site, (ii) the backward flux of water vapor released by the continent to the regional atmosphere, and (iii) possible modification of isotopic signatures of rainfall due to partial evaporation of raindrops and their interaction with ambient water vapor reservoir below the cloud base.

The overwhelming majority of moist air masses arriving at Rio Claro during summer have their source somewhere in the equatorial Atlantic and are subject to long rainout history extending over several thousand kilometers. Along this pathway those air masses interact with the Amazon rainforest. Intensive recycling of moisture leads to small continental gradient of δ values of rainfall across the Amazon basin (Salati et al., 1979; Rozanski et al., 1993) and elevated *d*-excess (Gat, J. R., & Matsui, 1991). While arriving at Rio Claro, those air masses are strongly depleted in heavy isotopes due to enhanced rainout over the second portion of their trajectory (after deflection of moist air masses from the Andes), but they maintain the elevated deuterium excess inherited through interaction of maritime moisture with the Amazon rainforest. Such air masses generate precipitation depleted in heavy isotopes, with high *d*-excess value, as observed over Rio Claro.

The analyzed convective events representing spring and autumn season have substantially shorter 10-day trajectories suggesting that atmospheric “pump” transporting moisture from the equatorial Atlantic to the Amazon basin is much weaker

or non-existing during this time of a year. Those short trajectories also suggest enhanced interaction with the surface of the continent. The backward flux of moisture from the surface to the atmosphere, generated in evapotranspiration processes apparently becomes the major source of moisture for rainfall occurring during spring and autumn in the region.

It is a generally accepted fact that transpiration process, at its steady state, is a non-fractionating process i.e. it returns the soil water pumped by the plants to the atmosphere without any discernible change of its isotopic composition (e. g. Cuntz et al., 2007; Flanagan et al., 1991; Dongmann and Nürnberg, 1974). In the study region we have distinct dry and wet period (cf. Fig.2d). If we assume that soil water accessible to plants has the isotopic characteristics equal to mean values of the four summer events discussed above (-68,67, -10,28, 13.5‰, for δ^2H, $\delta^{18}O$ and *d*-excess, respectively), than water vapour released to the regional atmosphere in the transpiration process will have the same isotopic signatures. Now, if we assume that this water vapour is lifted up by convection processes and reaches the condensation level, the isotopic composition of the first condensate can be easily calculated assuming isotope equilibrium between gaseous and liquid phase of water at the cloud:

$$\delta_L = \alpha_{eq}(1000 + \delta_V) - 1000 \quad (1)$$

where δ_L and δ_V signify delta values of liquid (condensate) and vapor phase, respectively, at isotopic equilibrium, whereas α_{eq} stands for equilibrium fractionation factor. Equilibrium fractionation factors for ^2H and ^{18}O were calculated using empirical expressions proposed by (Horita and Wesolowski, 1994). The assumed condensation temperature was equal 18^{o}C (cf. Tdw for spring and autumn events – Table 1). The calculated isotope characteristics of the first condensate are equal +12.2, -0.46 and 15.8‰, for δ^2H, $\delta^{18}O$ and *d*-excess, respectively. Large potential of the transpiration process in generation of isotopically enriched rainfall is clearly seen from the above exemplary calculation.

In addition to water vapor generated in the transpiration process, the backward vapor flux from the continent to the regional atmosphere will also include evaporation of surface water bodies located in the footprint area of the rainfall collection site. Evaporation of surface water bodies will generate vapor slightly depleted in heavy isotopes when compared to the source water subject to evaporation, and isotopic composition of this vapor will be located on the Local Evaporation Line (LEL), to the left-hand side of the Local Meteoric Water Line, thus exhibiting high *d*-excess values (e. g. Rozanski et al., 2001). The fact that the mean *d*-excess value of spring and autumn convective rainfall events analyzed in this study (ca. 19.1‰) is higher than that obtained for the mean isotopic composition of four analyzed summer events (ca. 13.5‰ - cf. discussion above) provides the evidence that the flux of water vapor to the regional atmosphere, a part of dominating contribution generated by the transpiration process (10-day mean evapotranspiration values of summer, spring and autumn events are equal 41mm, 31mm and 24mm, respectively), will also contain the fraction originating from surface water evaporation in the region.

3.4. Assessing the impact of below-cloud processes on the isotope characteristics of convective precipitation

The third factor which may contribute to the observed large differences between δ values of convective rainfall events sampled during summer months and those collected during spring and autumn, (ca. 8‰ for $\delta^{18}O$ and 70‰ for δ^2H), generated under similar thermal conditions in the region, is the possible modification of the isotopic signatures of raindrops due to their partial

evaporation and interaction with ambient water vapor reservoir below the cloud base level. This issue will be discussed below in some detail. As the isotopic composition of near-ground water vapour during the sampled rainfall events has not been measured, application of the interpreting framework for below-cloud effects on the isotopic characteristics of rainfall proposed by Graf et al. (2019) cannot be adopted here. Instead, a rough, semi-quantitative assessment of the impact of those effects in the context of the discussed isotope data will be presented below. The assessment will focus on two rainfall events sampled in summer: (i) 2020/02/10 night-time event, and (ii) 24/02/2021 day-time event.

Due to lack of appropriate data, a number of simplifying assumptions has to be made: (i) median values of isotope and meteorological parameters recorded for each analysed event (Table 1) will be used in the calculations, (ii) linear interpolation of air temperature and relative humidity between the cloud base level and the ground level will be adopted, (iii) it will be assumed that atmosphere is saturated with water vapour at the cloud base level (RH = 100%), and (iv) the reservoir of water vapour below the cloud base level is isotopically homogeneous.

Isotopic evolution of raindrops falling through unsaturated humid atmosphere beneath the cloud base level will be calculated using generally accepted conceptual framework for isotope effects accompanying evaporation of water into a humid atmosphere (Craig and Gordon, 1965; Horita et al., 2008). Isotopic evolution of an isolated water body (e.g. falling raindrop) evaporating into a humid atmosphere ca be described by the following equation (Gonfiantini, 1986):

$$\delta = \left(\delta_o - \frac{A}{B}\right) F^B + \frac{A}{B} \quad (2)$$

where

$$A = \frac{h_N \delta_A + \varepsilon_{kin} + \varepsilon_{eq}/\alpha_{eq}}{1 - h_N + \varepsilon_{kin}} \quad (3)$$

and

$$B = \frac{h_N - \varepsilon_{kin} - \varepsilon_{eq}/\alpha_{eq}}{1 - h_N + \varepsilon_{kin}} \quad (4)$$

Parameter F signify the remaining fraction of the evaporating mass of water (raindrop) while δ_A stands for the isotopic composition of ambient moisture. Initial and actual isotopic compositions of the evaporating water body, expressed in δ notation, are represented by δ_o and δ, respectively (expressed here as a fractions of unity). The meaning of the remaining parameters in equations (3) and (4) reads as follows:

h_N – relative humidity of ambient atmosphere, normalized to the temperature of the evaporating water body

α_{eq} – temperature-dependent equilibrium fractionation factors, derived from empirical equations proposed by Horita and Wesolowski (1994).

ε_{eq} – equilibrium fractionation coefficient. $\varepsilon_{eq} = \alpha_{eq} - 1$

ε_{kin} - kinetic fractionation coefficient. $\varepsilon_{kin} = \alpha_{kin} - 1$.

It can be shown (Gat, 2001; Horita et al., 2008) that kinetic fractionation coefficient is a linear function of the relative humidity deficit in the ambient atmosphere:

$$\varepsilon_{kin} = n \cdot \varepsilon_{diff}(1 - h_N) \quad (5)$$

where n stands for numerical factor, called turbulence parameter, varying in the range from zero to one, h_N signify relative humidity normalized to the temperature of the evaporating water body, whereas ε_{diff} is the kinetic fractionation coefficient associated with diffusion of water isotopologues in air.

The value of n is controlled mainly by wind conditions prevailing over the evaporating surface. It quantifies apparent reduction of the diffusive fractionation coefficient ε_{diff} due to impact of turbulent transport. The value of n = 0.5, was adopted in the calculations, following the results of laboratory experiments with evaporation of water drops in humid atmosphere reported by Steward (1975). The value of F parameter for each analyzed event was assessed based on the same publication (Stewart, 1975) (Fig. 4) assuming drop radius equal 1 mm. Travel time of raindrops drops from the cloud base to the surface was derived from the position of LCL level and the terminal velocity of drops, both reported for the analyzed events in Table 1. It was further assumed in the calculations that the difference between drop temperature and ambient air temperature is small, thus allowing to use ambient humidity instead to normalized humidity. Although this assumption may result in an over-estimation of the impact of partial evaporation of raindrops on their isotope characteristics, we think that the effect will be small hue to high ambient relative humidities (>90%) used in the calculations.

The results of the calculations outlined above are summarized in Table 2. It is clear that for atmospheric conditions prevailing during rainy period, represented by 2020/02/10 night-time convective event, the degree of partial evaporation of raindrops below the cloud base is negligible (reduction of the mean d-excess value in the order of 0.1‰). This stems mainly from the low elevation of the mean cloud level above the local ground and the resulting short travel time of raindrops to the surface, as well as very high relative humidity of ambient atmosphere below the cloud base. In contrast, the calculations preformed for the 24/02/2021 day-time event indicate that, for the situations with relatively high elevation of the cloud base level and low ambient relative humidity of the atmosphere beneath this level, the impact of partial evaporation of raindrops on their isotope characteristics can be substantial.

4 Concluding remarks

The results of this work provide deeper insights into the mechanisms controlling the isotopic variability of convective rainfall in the inland tropics of Brazil. High-frequency sampling of rainfall, covering a 1.5-year period (September 2019 – February 2021), was combined with extensive monitoring of meteorological parameters of the local atmosphere, satellite imagery and HYSPLIT backward trajectory modelling of moist air masses bringing rainfall the Rio Claro site, a continental, tropical location in the south-eastern Brazil. In total, 90 samples representing eight convective events covering three seasons (summer, autumn and spring) have been collected and analyzed.

On the monthly time scale, the Rio Claro site reveals typical variability observed in other tropical sites, with high amount of rainfall during the rainy period, strongly depleted in heavy isotopes, and high δ values during the dry period. The high-frequency isotope and meteorological data gathered in this study allowed to address the reasons of this strong seasonal variability of isotope characteristics of convective rainfall in some detail. The isotope characteristics of the analysed events

representing the rainy period, combined with dedicated Hysplit modelling of moist air masses associated with those events, suggest that overwhelming majority rainfall falling in south-eastern Brazil during austral summer is generated by moist air masses originating in the equatorial Atlantic Ocean. They pass the entire Amazon basin from east to west, interacting on the way with the rainforest through intense moisture recycling. Deflected by the Andes, they continue to the southeastern Brazil where they lose their high moisture load. It is hard to overestimate the importance of this regional atmospheric moisture transport scheme for the southeastern Brazil in the context of ongoing deforestation of the Amazon rainforest and progressing climate change. Possible weakening of the extent of moisture recycling over the Amazon rainforest may result in substantial reduction of precipitation amount in southeastern Brazil, with grave consequences for the Brazilian economy.

Peculiar isotope characteristics of the autumn and spring rainfall events analysed in this study, combined with dedicated Hysplit modelling of backward trajectories of moist air masses, strongly suggest that rainfall associated with the dry period in the region, largely originates from moisture of continental origin. This moisture flux is generated in evapotranspiration processes returning water stored in the soil column and in the surface water bodies predominantly during the rainy period. It should be emphasized that isotope characteristics of dry season rainfall provided a decisive argument in this respect.

Finally, thanks to high-resolution isotope and meteorological data generated in this study, the impact of purely local processes, such as below-cloud partial evaporation of raindrops on the isotopic composition of convective rainfall could be assessed. This semi-quantitative assessment confirmed that under specific conditions (high cloud base position in the local atmosphere, moderate or low relative humidity of ambient relative humidity of the atmosphere beneath this level), the impact of partial evaporation of raindrops on their isotope characteristics can be substantial.

Although high-frequency rainfall sampling is logistically difficult, we encourage future studies of this type in different geographical regions across the tropics, to better understand the factors controlling the isotopic composition of convective rainfall during rainy period. Such studies should be accompanied by extensive monitoring of local meteorological parameters and modelling of regional transport of moisture to the rainfall collection site.

Financial support

This work was funded by grants the São Paulo Research Foundation (FAPESP) under Processes 2018/06666-4, 2019/03467-3 and 2021/10538-4, and by the International Atomic Energy Agency Grant CRP-F31006.

Acknowledgment

FAPESP support for the scholarship provided under the Process 2019/03467-3 and 2021/10538-4 is acknowledged. Durán-Quesada acknowledges time for analysis and writing provided within UCR C1038 project.

References

Adler, R. F. and Fenn, D. D.: Thunderstorm Vertical Velocities Estimated from Satellite Data, American, 36, 1747–1754,

https://doi.org/10.1175/1520-0469(1979)036,1747: TVVEFS.2.0.CO;2., 1979.

Adler, R. F. and Mack, R. A.: Thunderstorm Cloud Top Dynamics as Inferred from Satellite Observations and a Cloud Top Parcel Model, American Meteorological Society, 43, 1945–1960, https://doi.org/10.1175/ 1520-0469(1986)043,1945:TCTDAI.2.0.CO;2, 1986.

Aemisegger, F. ., Spiegel, J. K. ., Pfahl, S. ., Sodemann, H. ., Eugster, W. ., and Wernli, H.: Isotope meteorology of cold front passages: A case study combining observations and modeling, Geophysical Research Letters, 42, 5652–5660, https://doi.org/10.1002/2015GL063988, 2015.

Aggarwal, P. K., Romatschke, U., Araguas-Araguas, L., Belachew, D., Longstaffe, F. J., Berg, P., Schumacher, C., and Funk, A.: Proportions of convective and stratiform precipitation revealed in water isotope ratios, Nature Geoscience, 9, 624–629, https://doi.org/10.1038/ngeo2739, 2016.

Barras, V. and Simmonds, I.: Observation and modeling of stable water isotopes as diagnostics of rainfall dynamics over southeastern Australia, Journal of Geophysical Research Atmospheres, 114, https://doi.org/10.1029/2009JD012132, 2009.

Celle-Jeanton, H., Gonfiantini, R., Travi, Y., and Sol, B.: Oxygen-18 variations of rainwater during precipitation: Application of the Rayleigh model to selected rainfalls in Southern France, Journal of Hydrology, 289, 165–177, https://doi.org/10.1016/j.jhydrol.2003.11.017, 2004.

Coplen, T. B., Neiman, P. J., White, A. B., Landwehr, J. M., Ralph, F. M., and Dettinger, M. D.: Extreme changes in stable hydrogen isotopes and precipitation characteristics in a landfalling Pacific storm, Geophysical Research Letters, 35, L21808, https://doi.org/10.1029/2008GL035481, 2008.

Craig, H. and Gordon, L. I.: Deuterium and oxygen 18 variations in the ocean and the marine atmosphere., edited by: Tongiorgi, E., Stable isotopes in oceanographic and paleotemperatures, Pisa, 9–130 pp., 1965.

Cuntz, M., Ogée, J., Farquhar, G. D., Peylin, P., and Cernusak, L. A.: Modelling advection and diffusion of water isotopologues in leaves, Plant, Cell and Environment, 30, 892–909, https://doi.org/10.1111/j.1365-3040.2007.01676.x, 2007.

Dansgaard, W.: Stable isotopes in precipitation, Tellus, 16, 436–468, https://doi.org/10.3402/tellusa.v16i4.8993, 1964.

Donat, M. G., Alexander, L. V., Yang, H., Durre, I., Vose, R., Dunn, R. J. H., Willett, K. M., Aguilar, E., Brunet, M., Caesar, J., Hewitson, B., Jack, C., Klein Tank, A. M. G., Kruger, A. C., Marengo, J., Peterson, T. C., Renom, M., Oria Rojas, C., Rusticucci, M., Salinger, J., Elrayah, A. S., Sekele, S. S., Srivastava, A. K., Trewin, B., Villarroel, C., Vincent, L. A., Zhai, P., Zhang, X., and Kitching, S.: Updated analyses of temperature and precipitation extreme indices since the beginning of the twentieth century: The HadEX2 dataset, Journal of Geophysical Research Atmospheres, 118, 2098–2118, https://doi.org/10.1002/jgrd.50150, 2013.

Dongmann, G. and Nürnberg, H. W.: On the Enrichment of H2180 in the Leaves of Transpiring Plants, Radiation and Environmental Biophysics, 52, 41–52, 1974.

Endries, J. L., Perry, L. B., Yuter, S. E., Seimon, A., Andrade-Flores, M., Winkelmann, R., Quispe, N., Rado, M., Montoya, N., Velarde, F., and Arias, S.: Radar-observed characteristics of precipitation in the tropical high andes of Southern Peru and Bolivia, Journal of Applied Meteorology and Climatology, 57, 1441–1458, https://doi.org/10.1175/JAMC-D-17-0248.1, 2018.

van der Ent, R. J. and Tuinenburg, O. A.: The residence time of water in the atmosphere revisited, Hydrology and Earth System Sciences, 21, 779–790, https://doi.org/10.5194/hess-21-779-2017, 2017.

Flanagan, L. B., Comstock, J. P., and Ehleringer, J. R.: Comparison of modeled and observed environmental influences on the stable oxygen and hydrogen isotope composition of leaf water in Phaseolus vulgaris L, Plant Physiology, 96, 588–596, https://doi.org/10.1104/pp.96.2.588, 1991.

Froehlich, K., Gibson, J. J., and Aggarwal, P.: Deuterium excess in precipitation and its climatological significance, Journal of Geophysical Research-Atmospheres, 1–23, 2002.

Gadgil, S.: The Indian monsoon and its variability, Annual Review of Earth and Planetary Sciences, 31, 429–467, https://doi.org/10.1146/annurev.earth.31.100901.141251, 2003.

García-Santos, S., Sánchez-Murillo, R., Peña-Paz, T., Chirinos-Escobar, M. J., Hernández-Ortiz, J. O., Mejía-Escobar, E. J., and Ortega, L.: Water stable isotopes reveal a complex rainfall to groundwater connectivity in central Honduras, Science of the Total Environment, 844, https://doi.org/10.1016/j.scitotenv.2022.156941, 2022.

Garreaud, R. D.: Cold air incursions over subtropical South America: Mean structure and dynamics, Monthly Weather Review, 128, 2544–2559, https://doi.org/10.1175/1520-0493(2000)128<2544:caioss>2.0.co;2, 2000.

Gat, J. R., & Matsui, E.: Atmospheric water balance in the Amazon Basin: An isotopic evapotranspiration model, Journal of Geophysical Research, 96, 13179–13188, https://doi.org/https://doi.org/10.1029/91JD00054, 1991.

Gat, J. R.: Environmental isotopes in the hydrological cycle: Principles and applications. Volume II, Atmospheric water, Technical documents in hydrology, Paris, 1–113 pp., 2001.

Gedzelman, S. D. and Lawrence, J. R.: The Isotopic Composition of Precipitatin from Two Extratropical Cyclones, American Meteorological Society, 118, 495–509, https://doi.org/10.1175/1520-0493(1990)118,0495: TICOPF.2.0.CO;2, 1990.

Gimeno, L., Drumond, A., Nieto, R., Trigo, R. M., and Stohl, A.: On the origin of continental precipitation, Geophysical Research Letters, 37, 1–7, https://doi.org/10.1029/2010GL043712, 2010.

Gimeno, L., Vázquez, M., Eiras-Barca, J., Sorí, R., Stojanovic, M., Algarra, I., Nieto, R., Ramos, A. M., Durán-Quesada, A. M., and Dominguez, F.: Recent progress on the sources of continental precipitation as revealed by moisture transport analysis, Earth-Science Reviews, 201, 103070, https://doi.org/10.1016/j.earscirev.2019.103070, 2020.

Gonfiantini, R.: Environmental isotopes in lake studies, in: Handbook of Environmental Isotope Geochemistry Vol. 2 The Terrestrial Environment, vol. 2, Elsevier, Amsterdan, 113–168, 1986.

Graf, P., Wernli, H., Pfahl, S., and Sodemann, H.: A new interpretative framework for below-cloud effects on stable water isotopes in vapour and rain, Atmospheric Chemistry and Physics, 19, 747–765, https://doi.org/10.5194/acp-19-747-2019, 2019.

Han, X., Lang, Y., Wang, T., Liu, C.-Q., Li, F., Wang, F., Guo, Q., Li, S., Liu, M., Wang, Y., and Xu, A.: Temporal and spatial variations in stable isotopic compositions of precipitation during the typhoon Lekima (2019), China, Science of The Total Environment, 762, 143143, https://doi.org/10.1016/j.scitotenv.2020.143143, 2021.

Horita, J. and Wesolowski, D. J.: Horita and Wesolowski 1994, Geochimica et Cosmochimica Acta, 58, 1–13, 1994.

Horita, J., Rozanski, K., and Cohen, S.: Isotope effects in the evaporation of water: a status report of the Craig–Gordon model, Isotopes in Environmental and Health Studies, 44, 23–49, https://doi.org/10.1080/10256010801887174, 2008.

Houze, R.: Stratiform precipitation in regions of convection: A Meteorological Paradox?, Bulletin of the American Meteorological Society, 78, 2179–2195, 1997.

Houze, R. A.: Cloud dynamics, Academic Press Limited, 573 pp., https://doi.org/10.1016/0377-0265(87)90017-0, 1993.

Houze, R. A.: Mesoscale Convective Systems, in: International Geophysics, vol. 104, 237–286, https://doi.org/10.1016/B978-0-12-374266-7.00009-3, 2004.

Houze, R. A. J.: Observed structure of mesoscale convective systems and implications for large-scale heating., Quart. J. Roy. Meteor. Soc., 115, 425–461, 1989.

Hu, J., Emile-Geay, J., Nusbaumer, J., and Noone, D.: Impact of Convective Activity on Precipitation δ18O in Isotope-Enabled General Circulation Models, Journal of Geophysical Research: Atmospheres, 123, 13,595-13,610, https://doi.org/10.1029/2018JD029187, 2018.

IAEA: IAEA / GNIP precipitation sampling guide V2.02, Global Network of Isotopes in Precipitation (GNIP), 20, 2014.

IPCC, W. G. I.-T. P. S. B.: Regional fact sheet – Central and South America, Sixth Assessment Report, 1–2 pp., 2021.

Jeelani, G., Deshpande, R. D., Galkowski, M., and Rozanski, K.: Isotopic composition of daily precipitation along the southern foothills of the Himalayas: Impact of marine and continental sources of atmospheric moisture, Atmospheric Chemistry and Physics, 18, 8789–8805, https://doi.org/10.5194/acp-18-8789-2018, 2018.

Klaassen, W.: Radar Observations and Simulation of the Melting Layer of Precipitation, Journal of the Atmospheric Sciences, 45, 3741–3753, 1988.

Kodama, Y.: Large-scale common features of subtropical precipitation zones (the Baiu Frontal Zone , the SPCZ , and the SACZ) Part I: Characteristics of subtropical frontal zones, Journal of the Meteorological Society of Japan, 70, 813–836, https://doi.org/10.1248/cpb.37.3229, 1992.

Kurita, N.: Water isotopic variability in response to mesoscale convective system over the tropical ocean, Journal of Geophysical Research Atmospheres, 118, 10,376-10,390, https://doi.org/10.1002/jgrd.50754, 2013.

Lawrence, J. R., Gedzelman, S. D., Dexheimer, D., Cho, H. K., Carrie, G. D., Gasparini, R., Anderson, C. R., Bowman, K. P., and Biggerstaff, M. I.: Stable isotopic composition of water vapor in the tropics, Journal of Geophysical Research-Atmospheres, 109, 16, https://doi.org/D0611510.1029/2003jd004046, 2004.

Lee, J. and Fung, I.: "Amount effect" of water isotopes and quantitative analysis of post-condensation processes, Hydrological Processes, 22, 1–8, https://doi.org/10.1002/hyp.6637, 2008.

Lekshmy, P. R., Midhun, M., Ramesh, R., and Jani, R. A.: 18 O depletion in monsoon rain relates to large scale organized convection rather than the amount of rainfall, Scientific Reports, 4, 1–5, https://doi.org/10.1038/srep05661, 2014.

Luiz Silva, W., Xavier, L. N. R., Maceira, M. E. P., and Rotunno, O. C.: Climatological and hydrological patterns and verified trends in precipitation and streamflow in the basins of Brazilian hydroelectric plants, Theoretical and Applied Climatology, 137, 353–371, https://doi.org/10.1007/s00704-018-2600-8, 2019.

Machado, L. A. T. and Rossow, W. B.: Structural Characteristics and Radiative Properties of Tropical Cloud Clusters, Monthly Weather Review, 121, 3234–3260, 1993.

Machado, L. A. T., Rossow, W. B., Guedes, R. L., and Walker, A. W.: Life cycle variations of mesoscale convective systems over the Americas, Monthly Weather Review, 126, 1630–1654, https://doi.org/10.1175/1520-0493(1998)126<1630:LCVOMC>2.0.CO;2, 1998.

Marengo, J. A., Soares, W. R., Saulo, C., and Nicolini, M.: Climatology of the low-level jet east of the Andes as derived from the NCEP-NCAR reanalyses: Characteristics and temporal variability, Journal of Climate, 17, 2261–2280, https://doi.org/10.1175/1520-0442(2004)017<2261:COTLJE>2.0.CO;2, 2004.

Marengo, J. A., Ambrizzi, T., Alves, L. M., Barreto, N. J. C., Simões Reboita, M., and Ramos, A. M.: Changing Trends in Rainfall Extremes in the Metropolitan Area of São Paulo: Causes and Impacts, Frontiers in Climate, 2, 1–13, https://doi.org/10.3389/fclim.2020.00003, 2020.

Mehta, S., Mehta, S. K., Singh, S., Mitra, A., Ghosh, S. K., and Raha, S.: Characteristics of the Z–R Relationships Observed Using Micro Rain Radar (MRR-2) over Darjeeling (27.05° N, 88.26° E): A Complex Terrain Region in the Eastern Himalayas, Pure and Applied Geophysics, 177, 4521–4534, https://doi.org/10.1007/s00024-020-02472-6, 2020.

Moerman, J. W., Cobb, K. M., Adkins, J. F., Sodemann, H., Clark, B., and Tuen, A. A.: Diurnal to interannual rainfall δ18O variations in northern Borneo driven by regional hydrology, Earth and Planetary Science Letters, 369–370, 108–119, https://doi.org/10.1016/j.epsl.2013.03.014, 2013.

Muller, C. L., Baker, A., Fairchild, I. J., Kidd, C., and Boomer, I.: Intra-Event Trends in Stable Isotopes: Exploring Midlatitude Precipitation Using a Vertically Pointing Micro Rain Radar, Journal of Hydrometeorology, 16, 194–213, https://doi.org/10.1175/JHM-D-14-0038.1, 2015.

Munksgaard, N. C., Zwart, C., Haig, J., Cernusak, L. A., and Bird, M. I.: Coupled rainfall and water vapour stable isotope time series reveal tropical atmospheric processes on multiple timescales, Hydrological Processes, 34, 111–124, https://doi.org/10.1002/hyp.13576, 2020.

Rao, N. T., Kirankumar, N. V. P., Radhakrishna, B., and Rao, N. D.: Classification of tropical precipitating systems using wind profiler spectral moments. Part I: Algorithm description and validation, Journal of Atmospheric and Oceanic Technology, 25, 884–897, https://doi.org/10.1175/2007JTECHA1031.1, 2008.

Ribeiro, B. Z., Machado, L. A. T., Biscaro, T. S., Freitas, E. D., Mozer, K. W., and Goodman, S. J.: An evaluation of the GOES-16 rapid scan for nowcasting in southeastern brazil: Analysis of a severe hailstorm case, Weather and Forecasting, 34, 1829–1848, https://doi.org/10.1175/WAF-D-19-0070.1, 2019.

Risi, C., Bony, S., Vimeux, F., Chongd, M., and Descroixe, L.: Evolution of the stable water isotopic composition of the rain sampled along sahelian squall lines, Quarterly Journal of the Royal Meteorological Society, 136, 227–242, https://doi.org/10.1002/qj.485, 2010.

Roberts, R. D. and Rutledge, S.: Nowcasting storm initiation and growth using GOES-8 and WSR-88D data, Weather and Forecasting, 18, 562–584, https://doi.org/10.1175/1520-0434(2003)018<0562:NSIAGU>2.0.CO;2, 2003.

Romatschke, U. and Houze, R. A.: Extreme summer convection in South America, Journal of Climate, 23, 3761–3791, https://doi.org/10.1175/2010JCLI3465.1, 2010.

Romatschke, U. and Houze, R. A.: Characteristics of precipitating convective systems accounting for the summer rainfall of tropical and subtropical South America, Journal of Hydrometeorology, 14, 25–46, https://doi.org/10.1175/JHM-D-12-060.1, 2013.

Rozanski, K., Sonntag, C., and Munnich, K. O.: Factors controlling stable isotope composition of European precipitation., Tellus, 34, 142–150, https://doi.org/10.3402/tellusa.v34i2.10796, 1982.

Rozanski, K., Araguás-Araguás, L., and Gonfiantini, R.: Isotopic Patterns in Modern Global Precipitation, 1–36, https://doi.org/10.1029/GM078p0001, 1993.

Rozanski, K., Mook, W. G., and Froehlich, K.: Environmental Isotopes in the Hydrological Cycle: Principles and Applications., Technical documents in hydrology, Paris, 1–117 pp., 2001.

Salati, E., Dall'Olio, A., Matsui, E., and Gat, J. R.: Recycling of water in the Amazon Basin: An isotopic study, Water Resources Research, 15, 1250–1258, https://doi.org/10.1029/WR015i005p01250, 1979.

Sánchez-Murillo, R., Durán-Quesada, A. M., Birkel, C., Esquivel-Hernández, G., and Boll, J.: Tropical precipitation anomalies and d-excess evolution during El Niño 2014-16, Hydrological Processes, 31, 956–967, https://doi.org/10.1002/hyp.11088, 2017.

Sánchez-Murillo, R., Durán-Quesada, A. M., Esquivel-Hernández, G., Rojas-Cantillano, D., Birkel, C., Welsh, K., Sánchez-Llull, M., Alonso-Hernández, C. M., Tetzlaff, D., Soulsby, C., Boll, J., Kurita, N., and Cobb, K. M.: Deciphering key processes controlling rainfall isotopic variability during extreme tropical cyclones, Nature Communications, 10, 1–10, https://doi.org/10.1038/s41467-019-12062-3, 2019.

dos Santos, V., Marshall Fleming, P., Henrique Mancini, L., Dalva Santos Cota, S., de Lima, G. B., Rodrigues Gomes, R., Kirchheim, R. E., Sanchéz-Murillo, R., and Gastmans, D.: Distinguishing the Regional Atmospheric Controls on Precipitation Isotopic Variability in the Central-Southeast Portion of Brazil, Advances in Atmospheric Sciences, 39, 1693–1708, https://doi.org/10.1007/s00376-022-1367-0, 2022.

dos Santos, V., Gastmans, D., and Sánchez-Murillo, R.: Isotope and meteorologic database of high-frequency sampling of convective rainfall events in Rio Claro, Brazil, https://doi.org/10.17632/kk3gs8zn4s.1, 2023.

Schmit, T. J., Griffith, P., Gunshor, M. M., Daniels, J. M., Goodman, S. J., and Lebair, W. J.: A closer look at the ABI on the goes-r series, Bulletin of the American Meteorological Society, 98, 681–698, https://doi.org/10.1175/BAMS-D-15-00230.1, 2017.

Schumacher, C. and Houze, R. A.: Stratiform rain in the tropics as seen by the TRMM precipitation radar, Journal of Climate, 16, 1739–1756, https://doi.org/10.1175/1520-0442(2003)016<1739:SRITTA>2.0.CO;2, 2003.

Siqueira, J. R., Rossow, W. B., Machado, L. A. T., and Pearl, C.: Structural characteristics of convective systems over South America related to cold-frontal incursions, Monthly Weather Review, 133, 1045–1064, https://doi.org/10.1175/MWR2888.1, 2005.

Sodemann, H.: Tropospheric transport of water vapour: Lagrangian and Eulerian perspectives, Swiss Federal Institute of Technology Zurich, 230 pp., 2006.

Soderberg, K., Good, S. P., O'connor, M., Wang, L., Ryan, K., and Caylor, K. K.: Using atmospheric trajectories to model the isotopic composition of rainfall in central Kenya, Ecosphere, 4, 1–18, https://doi.org/10.1890/ES12-00160.1, 2013.

Stein, A. F., Draxler, R. R., Rolph, G. D., Stunder, B. J. B., Cohen, M. D., and Ngan, F.: Noaa's hysplit atmospheric transport and dispersion modeling system, Bulletin of the American Meteorological Society, 96, 2059–2077, https://doi.org/10.1175/BAMS-D-14-00110.1, 2015.

Steiner, M. and Smith, J. A.: Convective versus stratiform rainfall: An ice-microphysical and kinematic conceptual model, Atmospheric Research, 47–48, 317–326, https://doi.org/10.1016/S0169-8095(97)00086-0, 1998.

Stewart, M. K.: Stable isotope fractionation due to evaporation and isotopic exchange of falling waterdrops: Applications to atmospheric processes and evaporation of lakes, Journal of Geophysical Research, 80, 1133–1146, https://doi.org/10.1029/JC080i009p01133, 1975.

Sun, C., Shanahan, T. M., and Partin, J.: Controls on the Isotopic Composition of Precipitation in the South-Central United States, Journal of Geophysical Research: Atmospheres, 124, 8320–8335, https://doi.org/10.1029/2018JD029306, 2019.

Sun, C., Tian, L., Shanahan, T. M., Partin, J. W., Gao, Y., Piatrunia, N., and Banner, J.: Isotopic variability in tropical cyclone precipitation is controlled by Rayleigh distillation and cloud microphysics, Communications Earth & Environment, 3, https://doi.org/10.1038/s43247-022-00381-1, 2022.

Taupin, J.-D., Gallaire, R., and Arnaud, Y.: Analyses isotopiques et chimiques des précipitations sahélienne de la région de Niamey au Niger: implications climatologiques, Hydrochemistry, 151–162, 1997.

Tharammal, T., G. Bala, and D. N.: Impact of deep convection on the isotopic amount effect in tropical precipitation, Journal of Geophysical Research Atmospheres, 122, 1505–1523, https://doi.org/10.1002/2016JD025555, 2017.

Tremoy, G., Vimeux, F., Soumana, S., Souley, I., Risi, C., Favreau, G., and Oï, M.: Clustering mesoscale convective systems with laser-based water vapor δ 18 O monitoring in Niamey (Niger), Journal of Geophysical Research: Atmospheres, 119, 5079–5103, https://doi.org/10.1002/2013JD020968, 2014.

Vila, D. A., Machado, L. A. T., Laurent, H., and Velasco, I.: Forecast and tracking the evolution of cloud clusters (ForTraCC) using satellite infrared imagery: Methodology and validation, Weather and Forecasting, 23, 233–245, https://doi.org/10.1175/2007WAF2006121.1, 2008.

Vuille, M., Bradley, R. S., Werner, M., Healy, R., and Keimig, F.: Modeling δ18O in precipitation over the tropical Americas: 1. Interannual variability and climatic controls, Journal of Geophysical Research: Atmospheres, 108, 1–24, https://doi.org/10.1029/2001JD002038, 2003.

Wang, T. and Tang, G.: Spatial Variability and Linkage Between Extreme Convections and Extreme Precipitation Revealed by 22-Year Space-Borne Precipitation Radar Data, Geophysical Research Letters, 47, 1–10, https://doi.org/10.1029/2020GL088437, 2020.

Winnick, M. J., Chamberlain, C. P., Caves, J. K., and Welker, J. M.: Quantifying the isotopic "continental effect," Earth and

Planetary Science Letters, 406, 123–133, https://doi.org/10.1016/j.epsl.2014.09.005, 2014.

Worden, J., Noone, D., Bowman, K., Beer, R., Eldering, A., Fisher, B., Gunson, M., Goldman, A., Herman, R., Kulawik, S. S., Lampel, M., Osterman, G., Rinsland, C., Rodgers, C., Sander, S., Shephard, M., Webster, C. R., and Worden, H.: Importance of rain evaporation and continental convection in the tropical water cycle, Nature, 445, 528–532, https://doi.org/10.1038/nature05508, 2007.

World Meteorological Organization: WMO Atlas of Mortality and Economic Losses From Weather , Climate and Water Extremes (1970-2019), Geneva 2, Switzerland, 90 pp., 2021.

Zilli, M. T., Carvalho, L. M. V., Liebmann, B., and Silva Dias, M. A.: A comprehensive analysis of trends in extreme precipitation over southeastern coast of Brazil, International Journal of Climatology, 37, 2269–2279, https://doi.org/10.1002/joc.4840, 2017.

Zwart, C., Munksgaard, N. C., Lambrinidis, D., Bird, M. I., Protat, A., and Kurita, N.: The isotopic signature of monsoon conditions , cloud modes , and rainfall type, Hydrological Processes, 2296–2303, https://doi.org/10.1002/hyp.13140, 2018.

Table 1. Summarizing overall convective rainfall events and median values of isotope and meteorological parameters.

Season	Daytime	Data	Number of samples	Duration	Isotopes			Automatic Weather Station					Micro Rain Radar		GOES-16
					$\delta^{18}O$	$\delta^{2}H$	*d*-excess	Rain rate	RH	T	Tdw	LCL	Z	w	BT
			n	minutes	‰			$mm.min^{-1}$	%	°C		meters	dBZ	$m.s^{-1}$	°C
Spring	Day	05/11/2019	21	82	-3.1	0.8	22.9	0.4	96	21	20	146	46	8.0	-63
Spring	Day	18/11/2020	8	141	-4.2	-13.7	19.7	0.2	86	20	17	489	38	7.1	-63
Autumn	Day	09/06/2020	12	96	-3.4	-5.6	17.3	0.3	95	19	18	168	42	7.7	-50
Autumn	Night	23/05/2020	4	131	-2.9	-6.9	16.3	0.0	87	19	17	449	33	6.6	-56
Summer	Night	30/01/2020	6	23	-10.0	-64.4	15.7	0.4	93	23	21	247	38	6.6	-53
Summer	Night	10/02/2020	18	86	-13.9	-92.0	17.5	0.5	97	22	21	93	41	6.7	-39
Summer	Day	01/02/2020	5	18	-10.4	-73.5	13.4	0.6	93	23	21	253	39	7.1	-60
Summer	Day	24/02/2021	16	55	-6.8	-44.8	7.2	0.5	86	21	18	468	35	7.1	-51

RH = Relative Humidity, T = Temperature, Tdw = Dew point temperature, LCL = Lifting condensation level, Z = Reflectivity, w = fall velocity and Brightness temperature.

Table 2. The results of semi-quantitative assessment of the *i*mpact of below-cloud processes on the isotope characteristics of convective precipitation

Rainfall event	T_{INT} a) (ºC)	RH_{INT} b) (%)	F c) (-)	Δd-excess d) (‰)
The 10/02/2020 event	21.7	98.6	0.9994	0.1
δ_o - isotopic composition of rainfall (‰):				
δ^2H = -91.97, $\delta^{18}O$ = -13.85, *d*-excess = 18.8				
δ_A – isotopic composition of equilibrium vapour (‰) e):				
δ^2H = -161.6 $\delta^{18}O$ = -23.28, *d*-excess = 24.6				
The 24/02/2021 day-time event	19.3	93.2	0.9800	3.0
δ_o - isotopic composition of rainfall (‰):				
δ^2H = -44.8, $\delta^{18}O$ = -6.79, *d*-excess = 9.5				
δ_A – isotopic composition of equilibrium vapour (‰):				
δ^2H = -120.3 $\delta^{18}O$ = -16.48, *d*-excess = 11.5				

a) mean temperature of below cloud ambient atmosphere (linear interpolation between cloud base and ground level values)
b) mean relative humidity of below cloud ambient atmosphere (linear interpolation between cloud base and ground level values)
c) remaining mass fraction of raindrops after their travel from the cloud base to the surface (see text)
d) reduction of the d-excess of raindrops as a result of their travel from the cloud base to the surface (see text)
e) assumed isotopic composition of ambient humid atmosphere below the cloud base derived from the measured isotopic composition of rainfall and ground-level temperature.

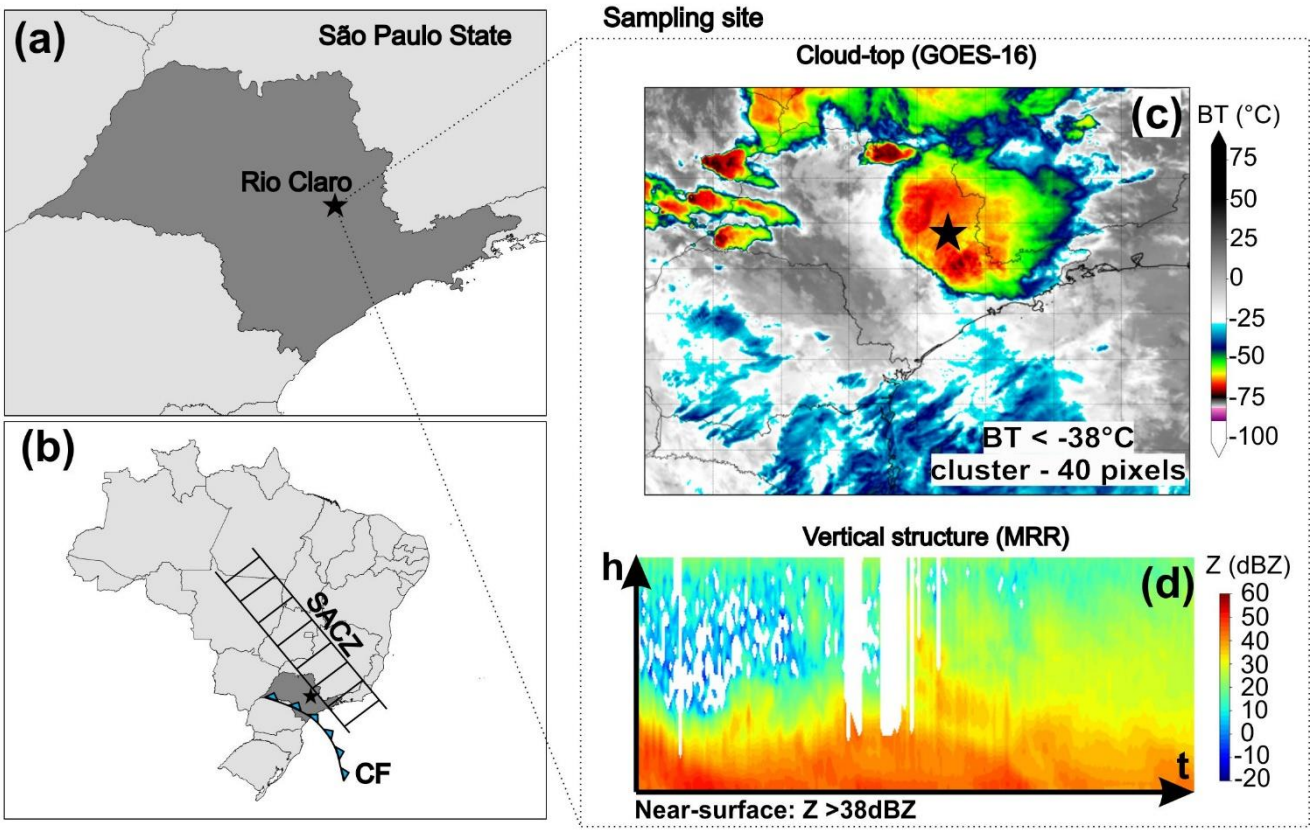

Figure 1. (a) Localization of sampling site in Rio Claro (black star) (b) in regional synoptic context across Brazil and main weather systems (CF – cold front and SACZ – Southern Atlantic Convergence Zone). Over collection point (c) GOES-16 satellite imagery showed convective system with lower brightness temperature (BT, clou-top) and (d) Micro Rain Radar (MRR) illustrates the vertical structure of convective rainfall, height (h) and time (t), characterized by radar reflectivity (Z) with strong values near-surface.

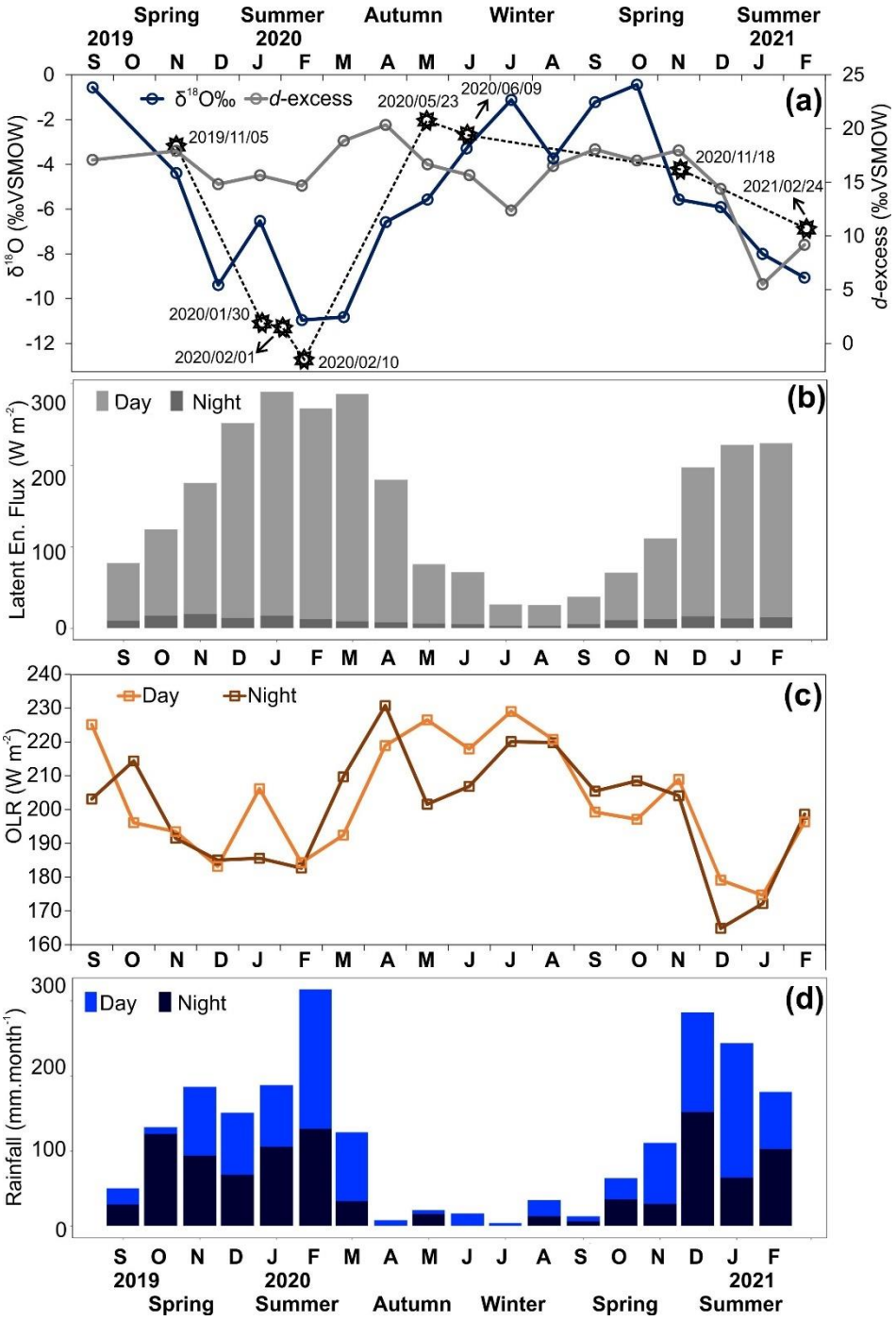

Figure 2. (a) Seasonal variation of $\delta^{18}O$ and *d*-excess values in monthly rainfall and aggregated monthly $\delta^{18}O$ values high-frequency convective rainfall sampling discussed in this study (b) AQUA/AIRS latent heat flux. (c) MERRA-2 outgoing longwave radiation (monthly averaged daytime and night-time data) (d) monthly rainfall amounts at Rio Claro separated into day and night fraction (no rainfall types distinguished). The star symbol indicates the collected high-frequency events, ranked according to average values of $\delta^{18}O$.

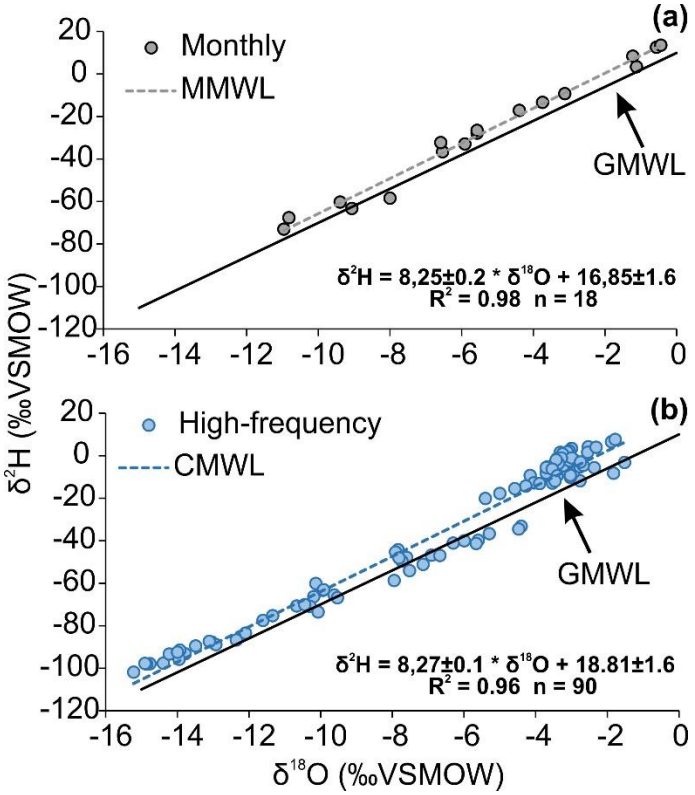

Figure 3. (a) Monthly and (b) high-frequency δ^2H and $\delta^{18}O$ rainfall data plotted in the $\delta^2H/\delta^{18}O$ space. LMWL – local meteoric water line based on monthly values, CMWL – convective meteoric water line and GMWL – global meteoric water line.

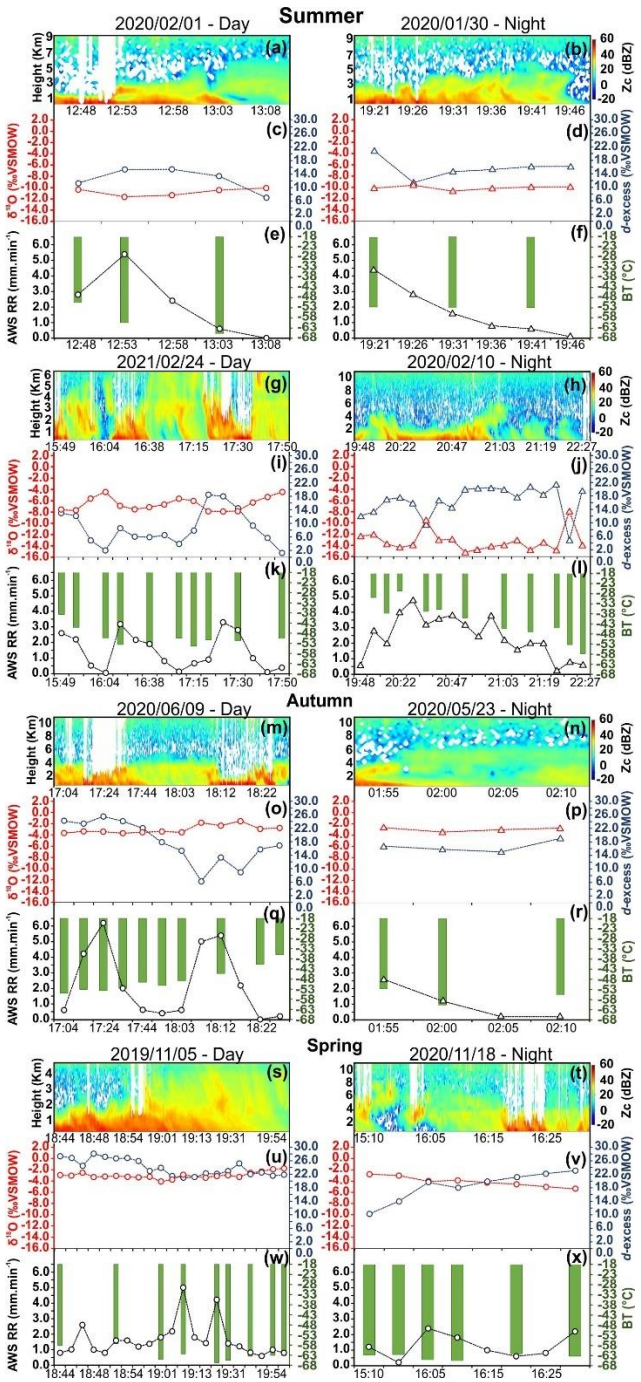

Figure 4. Intra-event variability of eight convective rainfall sampling. For summer season, 2020/02/01(a, c, e), 2020/01/30 (b, d, f), 24/02/21 (g, i, k) and 2020/02/10 (h, j, l), autumn, 09/06/2020 (m, o, q) and 23/05/2020 (n, p, r), autumn 05/11/2019 (s, u, w) and 18/11/2020 (t, v, x). $\delta^{18}O$ is red color, *d*-excess is orange, rain rate (RR) in dark blue, brightness temperature (BT) in green. The Zc is the corrected reflectivity of Micro Rain Radar plotted as vertical profile.

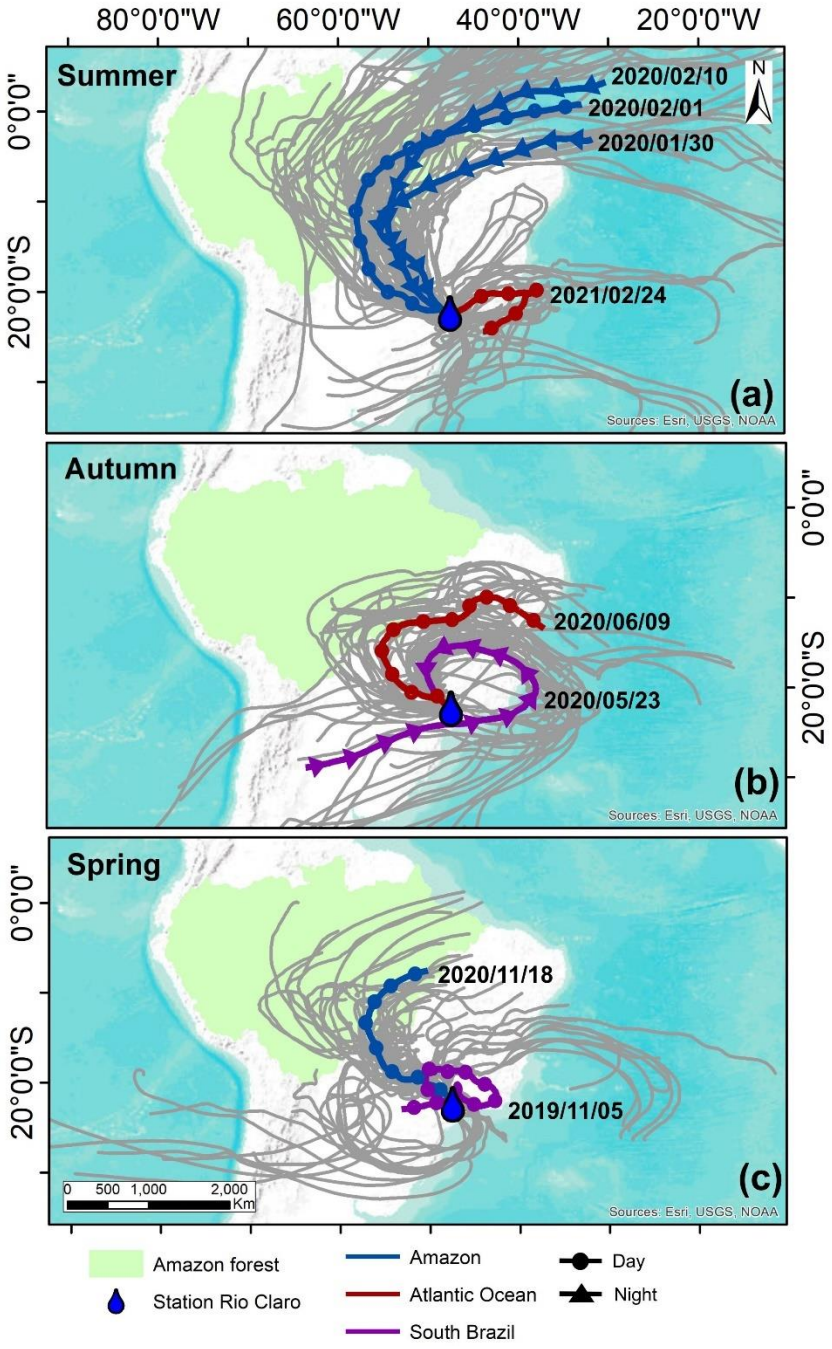

Figure 5. Ten-day backward trajectories arriving at Rio Claro station of eight convective events on (a) Summer, (b) Autumn and (c) Spring. Twenty-seven ensembles are grey lines, and the mean trajectory is the colors lines. The colours of the mean trajectories indicate the origin of air masses: blue influenced by Amazon Forest, Tuscan red from Atlantic Ocean and Purple from South Brazil portion. Symbols are daytime of convective events, day (circle) and night (triangle). The authors used trivial information, the borders of the countries and the ocean provided by the ESRI base map.

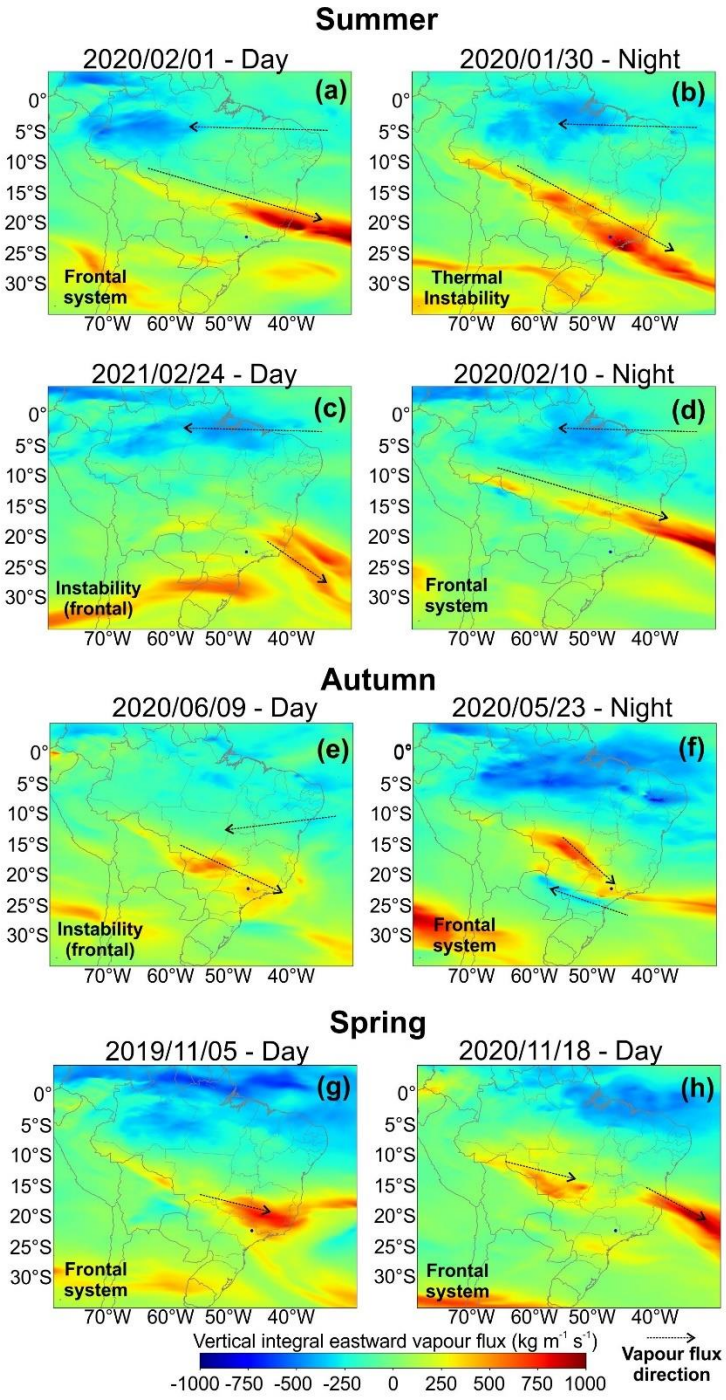

Figure 6. ERA-5 vertical integral of eastward water vapor flux for the days when convective rainfall events occurred, during (a, b, c, d) summer, (e, f) autumn and (g, h) spring aggregated with weather systems text. Positive values indicate the direction of moisture vapor flux from left to right, and negative values from right to left. Arrows illustrate the direction of vapour flux. The weather systems are indicated for each rainfall event.